anomalous scatterers is known, a somewhat less-accurate result is obtained from use of the simple system of equations despite the fact that the number of unknown quantities remains the same. The reason for this is the need to use a quadratic equation in addition to the linear ones, giving a twofold ambiguity which is accurately resolved by isomorphous-replacement data, but somewhat less accurately so with use of the known structure of the anomalous scatterers.

Another question concerning the system of algebraic equations concerns whether greater accuracy is obtained in the calculation of the phase differences when exact values of the structure factors for the anomalous scatterers are used, as obtained from their known structure, rather than the statistical values defined in (13). As seen in Table 4, it is better to use the statistical values of the structure-factor magnitudes when significant errors are present in the data.

Finally, the question concerning whether (20) and (21) could be used with rather accurate statistical estimates of $|F_{\mathbf{h}}^n|$ from (23) to give more accurate values for phase differences than alternative algebraic calculations is answered in Table 5. The accuracy of the values is about the same as that obtained in alternative systems of equations. It is also obvious from Table 5 that more-accurate values of $|F_{\mathbf{h}}^n|$ would lead to potentially accurate values for phase differences. More-accurate values for $|F_{\mathbf{h}}^n|$ would come from experiments that included shorter wavelengths.

This article has been devoted, for the most part, to one-wavelength anomalous-dispersion data. It has revealed some further characteristics of the information available which imply that, for some systems, a one-wavelength experiment may suffice to yield a solution. This is already known to be true from experience. It would seem, however, that unless it is quite expedient to work with one-wavelength data, the addition of isomorphous-replacement and multiple-wavelength information would be quite beneficial.

I thank Mr Stephen Brenner for writing the programs and making the computations reported here.

This work was supported in part by the Office of Naval Research and by USPHS grant GM 30902.

References

HAO, Q. & WOOLFSON, M. M. (1989). *Acta Cryst.* A**45**, 794-797.
HENDRICKSON, W. A. & TEETER, M. M. (1981). *Nature (London)*, **290**, 107-113.
KARLE, J. (1980). *Int. J. Quantum Chem.* **7**, 357-367.
KARLE, J. (1984). *Acta Cryst.* A**40**, 1-4.
KARLE, J. (1985*a*). *Acta Cryst.* A**41**, 182-189.
KARLE, J. (1985*b*). *Acta Cryst.* A**41**, 387-394.
KARLE, J. (1986). *Acta Cryst.* A**42**, 246-253.
KARLE, J. (1989). *Acta Cryst.* A**45**, 303-307.
OKAYA, Y., SAITO, Y. & PEPINSKY, R. (1955). *Phys. Rev.* **98**, 1857-1858.
SHOTTON, D. M. & WATSON, H. C. (1970). *Nature (London)*, **225**, 811-816.
TIMKOVITCH, R. & DICKERSON, R. E. (1976). *J. Biol. Chem.* **251**, 4033-4046.
WANG, B. C. (1985). In *Diffraction Methods in Biological Macromolecules*, edited by H. WYCKOFF, pp. 90-112. New York: Academic Press.
WATSON, H. C., SHOTTON, D. M., COX, J. M. & MUIRHEAD, H. (1970). *Nature (London)*, **225**, 806-811.

Acta Cryst. (1991). A**47**, 543-549

Continuous Diffuse Scattering from Polymethylene Chains – an Electron Diffraction Study of Crystalline Disorder

BY DOUGLAS L. DORSET AND HENGLIANG HU

Electron Diffraction Department, Medical Foundation of Buffalo, Inc., 73 High Street, Buffalo, NY 14203, *USA*

AND J. JÄGER

Abteilung Elektronenmikroskopie, Fritz-Haber-Institut der Max-Planck-Gesellschaft, Faradayweg 4-6, *D*-1000 *Berlin* 33, *Germany*

(*Received* 24 *January* 1991; *accepted* 26 *March* 1991)

Abstract

Continuous diffuse scattering is noted in electron diffraction patterns from polymethylene compounds such as *n*-paraffins and polyethylene. In a projection down the chain axes, experimentally produced by solution crystallization, the diffuse scatter in *hk*0 patterns disappears at low temperature, in accord with a thermal-diffuse-scattering model, which explains the intensity distribution and its temperature dependence. For a projection onto the chain axes, experimentally achieved by epitaxic orientation on benzoic

0108-7673/91/050543-07$03.00

acid crystals, the $0kl$, as well as 3D projections, contain diffuse scatter which does not disappear at low temperature. Its origin appears to be due to frozen-in longitudinal chain static displacements, perhaps as much as 0·25 Å, as indicated by a model for this disorder.

Introduction

Although the atomic positions in perfect crystals of polymethylene chain compounds are important for understanding preferred crystallization modes, and hence the phenomenon of polymorphism (*e.g.* Abrahamsson, Dahlén, Löfgren & Pascher, 1978), many of the important physical properties of molecular compounds containing an alkane chain moiety actually depend on the aggregation and dynamics of disordered atomic positions within the conformational constraints allowed for these zig-zag segments. The structure of liquid crystals is an extreme example where various kinds of chain disorder are accommodated, even though the average chain axis can have (more or less) a common orientation.

When a paraffin crystal is heated to the temperature where the solid–solid transition from orthorhombic to hexagonal 'rotator' phase occurs, the smaller dimensional scale for chain-packing disorder may, nevertheless, furnish some clues about liquid-crystalline phases. Powder X-ray crystallographic experiments (Asbach, Geiger & Wilke, 1979; Craievich, Doucet & Denicolo, 1984) have shown us that the major influence on the Bragg scattering is an attenuation of 'lamellar' intensity resolution due to the imperfection of the layer repeat. From electron-diffraction measurements on epitaxically oriented single microcrystals, it is seen that the implied perturbations at the lamellar interface do not appreciably affect the scattering from the polymethylene sublattice (Dorset, Moss, Wittmann & Lotz, 1984). Unfortunately, because of the small number of measurements, it was not possible to determine a model for the chain-packing defects solely from the Bragg intensity data. Vibrational spectroscopy has been a more valuable tool for this purpose. Using selectively deuterated short odd-chain alkanes which undergo the 'rotator' transition, Maroncelli and co-workers (Maroncelli, Qi, Strauss & Snyder, 1982; Maroncelli, Strauss & Snyder, 1985) were able to determine that most 'kink' defects in the heated alkane molecules were concentrated near the chain ends. A model based on the Dill–Flory (1980, 1981) lattice representation of lipid chain defects was found to fit the experimental data very well if an additional longitudinal translational disorder were included (Maroncelli, Strauss & Snyder, 1985). Later, similar types of kink populations were found for the higher *n*-paraffins which do not undergo a 'rotator' phase transition before the melt (Kim, Strauss & Snyder, 1989).

It is clear that the best diffraction probe of chain disorder is not the Bragg scattering but the continuous diffuse scatter which connects these diffraction peaks (Guinier, 1963). In order to account for the rather intense continuous diffraction from epitaxically crystallized polymethylene chain compounds (Dorset, Moss, Wittmann & Lotz, 1984), an attempt was made to construct a defect model which would explain both the location and intensity of this diffuse signal. The analysis (Dorset, Moss & Zemlin, 1985–1986) was partially successful by matching the reciprocal-space locations for the diffuse intensity, although kink defects produced the same qualitative result as thermal motion. It was decided that the former origin would be preferred since this defect scattering persists to very low temperatures (*e.g.* 10 K). Nevertheless, the match to the observed scattering-intensity distribution was not satisfactory in that both models resulted in a reversed order of its distribution.

This paper is a more complete description of the disordered packing of polymethylene chains, showing, first of all, which modes are most important for explaining the continuous diffuse scatter and, secondly, which is most dependent upon temperature. For these studies we use data from epitaxically and solution-crystallized materials, thus affording orthogonal views of the chain packing.

Materials and methods

Solution crystallization of the *n*-paraffins *n*-$C_{33}H_{68}$ and *n*-$C_{36}H_{74}$ (Fluka AG, Buchs, Switzerland) was carried out by evaporation of a dilute solution in light petroleum onto a carbon-covered electron-microscope grid. For epitaxic orientation, the light-petroleum solution was first evaporated to dryness onto a cleaved mica sheet. After placing carbon-covered electron-microscope grids face down over areas containing the paraffin, an excess of benzoic acid crystals was added at their perimeters and a physical sandwich made with another mica sheet. This sandwich is first heated to solubilize the *n*-paraffin in the molten benzoic acid and then cooled to freeze out the eutectic solid. The procedure is basically the same as described by Wittmann, Hodge & Lotz (1983) and the epitaxic orientation is understood in the context of the binary phase diagram (Dorset, Hanlon & Karet, 1989). A sample of polyethylene was epitaxically oriented in a similar fashion except that the microcrystals were annealed at 353 K in the presence of the benzoic acid substrate for 30 min to improve the polymer crystallinity (Hu & Dorset, 1989). (Nevertheless, there is still some polycrystalline disorder as evidenced by the arc-like appearance of some diffraction spots.)

Transmission electron-diffraction experiments were carried out at 100 kV, taking extreme care that beam dosages were low enough to minimize radiation

damage to the specimen. This is a very important consideration since the change in Bragg scattering due to beam damage is quite similar to the thermally induced changes (Dorset, Holland & Fryer, 1984). In Buffalo, a JEOL-JEM-100B electron microscope was used and diffraction patterns recorded on Kodak DEF-5 X-ray film. With a Gatan 626 liquid-nitrogen cooling stage, it is possible to observe diffraction patterns at temperatures from ambient down to 100 K. In Berlin, either the Deeko 250 or Suleika electron microscopes were used which can cool specimens, respectively, to 40 or 4 K. In these instruments, patterns were recorded on Agfa 23D56 at a shorter camera length than used in Buffalo (since the film grain is finer).

Theory

In order to account for the diffuse-scattering signals in the recorded electron-diffraction pattern, several possible contributions have to be considered which may be due to either thermal excitation of the space lattice or static disorder. Although we rely largely upon expressions given in previously published works, certain specific derivations were necessary for some cases which will be treated by one of us (HH) in a separate publication.

Thermal scattering

Thermal diffuse scatter (TDS) is an interaction of the incident beam with lattice phonons. Although, in principle, it is an inelastic process, the amount of energy exchanged is generally very small. Heidenreich (1964), for example, states that the largest phonon energy for aluminium is 0·03 V compared to the 10^5 V acceleration potential of the electron source used in our experiments. One is thus justified in regarding the phenomenon as approximately elastic and modeled by Gaussian disorder of the first kind (Vainshtein, 1966).

The TDS model employed here is taken from Amorós & Amorós (1968), *i.e.*

$$I_{\mathrm{TDS}}(\mathbf{r}^*) = \sum_{p=1}^{P} I_{p_0}(\mathbf{r}^*)\{1-\exp[-\tfrac{1}{2}B(\mathbf{r}^*)^2]\}. \qquad (1)$$

Here we assume that $I_{p_0}(\mathbf{r}^*)$ is the intensity transform of a molecule or coherently scattering unit at rest, where B is the isotropic temperature factor.

Defect scattering

Three sources of chain defects are considered, *i.e.* kinks, torsional distortions and longitudinal chain shifts. For kinks we employ Cochran's (1956) model for this defect which assumes that the kinks are isolated from one another. (Since they are located near the chain ends, this can be justified.) The diffuse intensity is therefore a variation of the Laue equation, *viz*

$$I_{\mathrm{kink}}(\mathbf{r}^*) = n\Big|\sum_m \{f'_m \exp[i2\pi\mathbf{r}'_m\cdot\mathbf{r}^*] - f_m \exp[i2\pi\mathbf{r}_m\cdot\mathbf{r}^*]\}^2\Big|. \qquad (2)$$

Here n is the number of kink segments in the disordered crystal. The atomic scattering factors f', f, respectively, represent atoms at displaced $\mathbf{r}'_m$ or undisplaced $\mathbf{r}_m$ positions. Kink coordinates were obtained from either of two crystal structures (Craven & Guerina, 1979; Dorset, Holland & Fryer, 1984; Dorset, Moss, Wittmann & Lotz, 1984), in which the defect geometries are similar to one another, or from a theoretical model (Boyd, 1975).

Torsional distortions are considered to involve C-atom positions perpendicular to the chain direction and it is assumed that adjacent chains may or may not have coupled motions. For uncorrelated torsional distortion, the result is very similar in form to (1).

Longitudinal displacements are modeled by a Gaussian static displacement model for the chains. Hence, similar to (1),

$$I_{\mathrm{longitudinal}}(\mathbf{r}^*) = |F|^2\{1-\exp[-4\pi^2 l^2\sigma_L^2]\}, \qquad (3)$$

where σ_L is the average molecular shift and l refers to the methylene subcell index along the $c_s = 2{\cdot}54$ Å axis. This model assumes that the chain displacements are uncorrelated.

Results

Electron-diffraction patterns from epitaxically oriented *n*-paraffins and polyethylene are shown in Fig. 1. Although the three compounds have different crystal structures, the diffuse diffraction lies at similar locations in reciprocal space with a consistent intensity distribution. It is obvious, therefore, that its origin is due to the polymethylene chain packing which is identical for all three structures. Using the methylene subcell indices $(0kl)_s$, the bands of diffuse scattering are projections of integral reciprocal planes, with the most intense bands at $l=2$ and the band at $l=0$ almost absent. Low-temperature experiments (Figs. 1*d*,*e*) indicate, as shown previously (Dorset, Moss & Zemlin, 1985–1986), that the continuous scatter is not appreciably affected by cooling of the specimen, except that the contribution to $l=0$ is weaker.

Although TDS is obviously not the principal cause of this diffuse signal, a calculation based on isotropic thermal motion [(1)] was carried out (Fig. 2*a*) to show that the intensity distribution is the reverse of the observed data in Fig. 1. The same discrepancy can be found if a kink model is used (Fig. 2*b*) as in (2), regardless of the atomic coordinates used for the defect site. Torsional disorder produces a similar

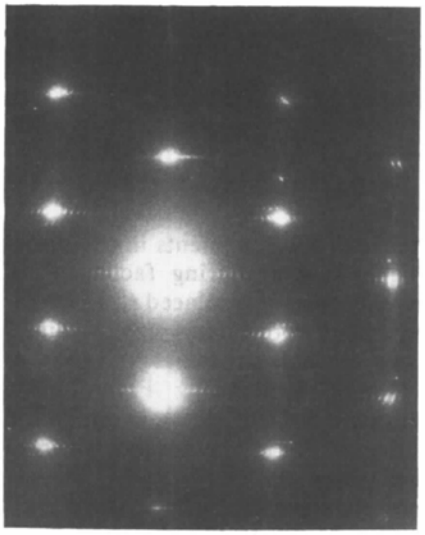

(*a*)

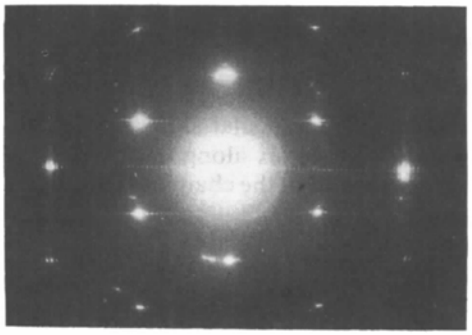

(*b*)

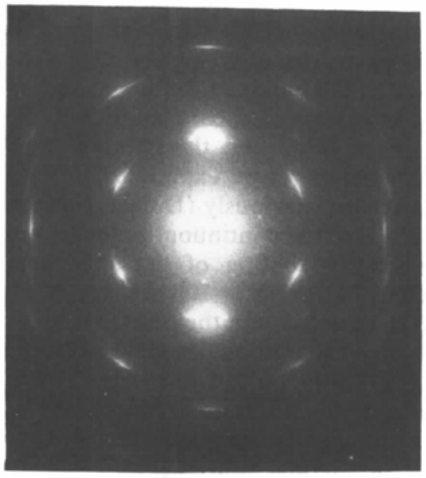

(*c*)

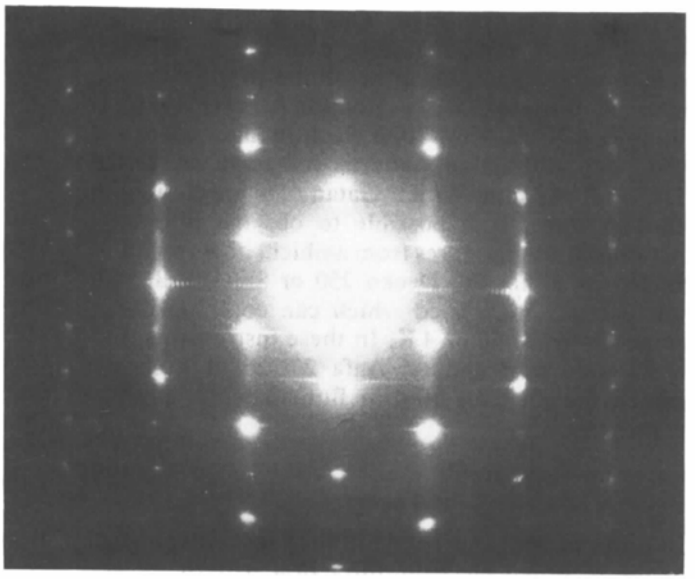

(*d*)

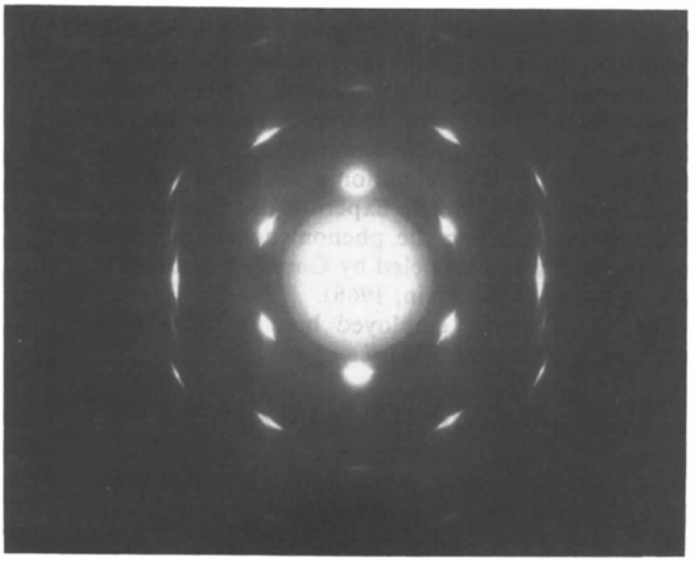

(*e*)

Fig. 1. Electron-diffraction patterns from epitaxically oriented polymethylene chain crystals. In these 0*kl* patterns from (*a*) *n*-$C_{33}H_{68}$, (*b*) *n*-$C_{36}H_{74}$ and (*c*) polyethylene, taken at room temperature, the bands of continuous diffuse scatter are superimposed on the Bragg diffraction. When the samples are cooled, *e.g.* (*d*) *n*-$C_{36}H_{74}$ at 15 K and (*e*) polyethylene at 40 K, the continuous scatter is still present except that the intensity at $l = 0$ is consistently weakened or absent.

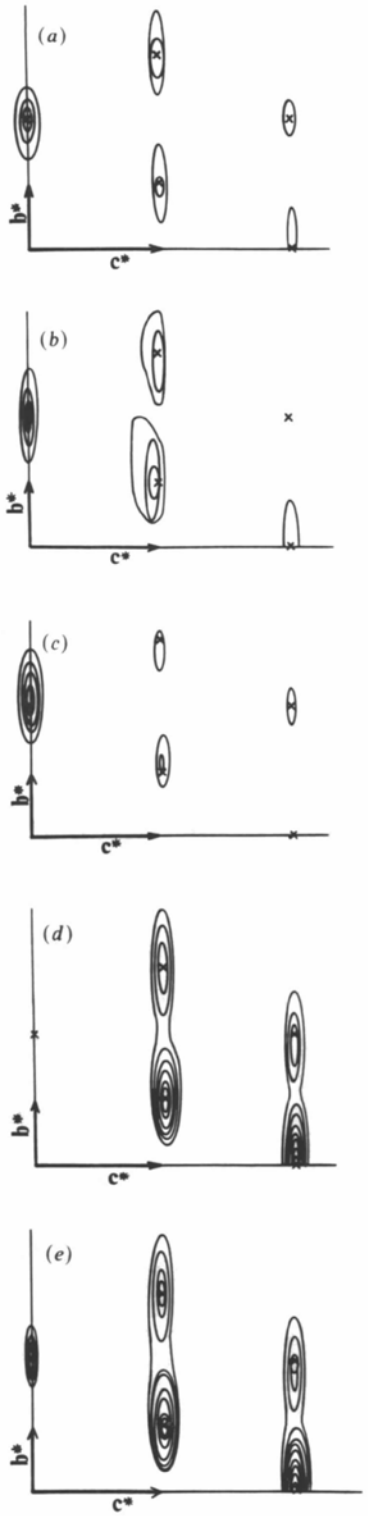

Fig. 2. Models for the observed diffuse scatter in Fig. 1: (*a*) TDS with $B = 3$ Å^2; (*b*) kink model; (*c*) torsional model. Note that these models explain the location of the diffuse signal but not its relative intensity. (*d*) A model based on longitudinal chain shifts fits the observed data; (*e*) if thermal motion is added, some intensity on the band at $l = 0$ appears.

signal (Fig. 2*c*) with the same reversed intensity distribution.

The best match to the observed 0*kl* diffuse scatter is due to longitudinal chain disorder, *e.g.* with $\sigma_L = 0{\cdot}1$ in (4). If only a static displacement is used, then the intensity at $l = 0$ is zero (Fig. 2*d*). Weak scattering can be placed at this reciprocal plane by including a slight thermal component (Fig. 2*e*), consistent with the apparent temperature sensitivity of this line indicated by the experimental results in Fig. 1. A further match can be made to the three-dimensional data from these crystals. For example, calculations based on (3) with incorporated thermal motion provide a good match to experimental three-dimensional data from polyethylene as well as *hkl* data from *n*-$C_{33}H_{68}$. The match to the *hhl* data from the paraffin is shown in Fig. 3.

In the orthogonal direction down the long chain axes, the *hk*0 diffuse signal from *n*-$C_{36}H_{74}$ is found

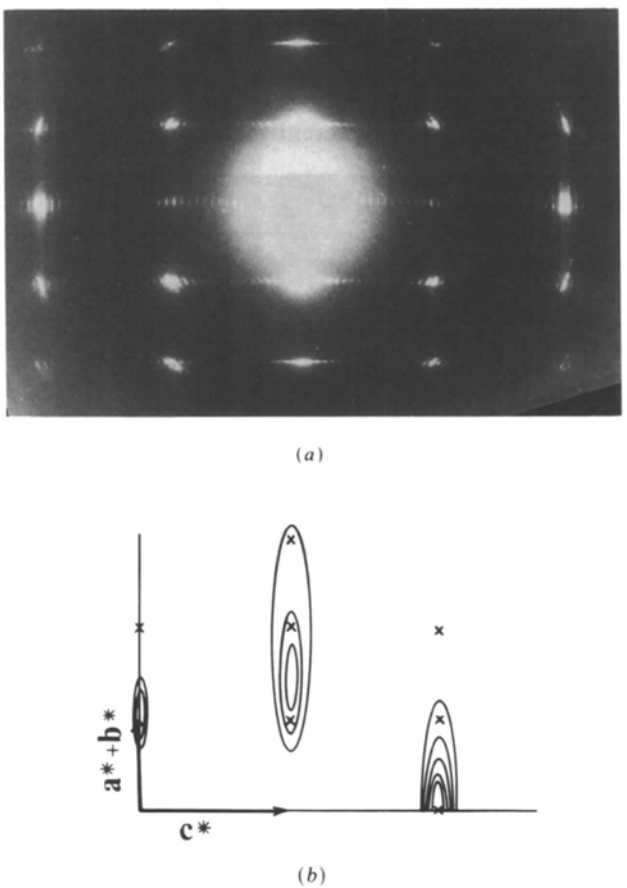

Fig. 3. Model calculations were carried out for three-dimensional diffuse scattering from polymethylene chains. For polyethylene, one can match the observed *lkl*, *hkl* and $k+l,k,l$ diffuse scatter with the computational model based upon longitudinal chain shifts. The fit of the model for *hhl* data is also shown by comparing the experimental data from *n*-$C_{33}H_{68}$ (*a*) with the calculation (*b*).

to be temperature sensitive (Fig. 4*a*,*b*), consistent with the results given above for $l = 0$. The most intense diffuse scatter, corresponding to the experimental data, is calculated from (1) (Fig. 4*c*). Although the results of the kink defect and correlated torsional modes are qualitatively similar, the low kink population and small torsional distortion (3–6°) would not contribute a large enough diffuse-scattering signal to be of any consequence.

Discussion

As shown above, low-temperature electron-diffraction experiments are useful for determining the source of continuous diffuse scatter connecting Bragg spots in patterns from linear polymethylene chain compounds. Projecting down the long chain axes, the diffuse scatter is found mainly to be due to thermal motion, since it is virtually extinguished for low-temperature specimens. This observation is in agreement with computations, since a TDS model leads to a satisfactory match of the experimental data. Consistent with earlier findings (Dorset, 1977), the best agreement occurs when the total unit-cell contents are used as the coherently scattering entity, a result contradicting the incoherently scattering molecules often employed by Amorós & Amorós (1968) or Hoppe (1964) in models for diffuse scatter from molecular organic crystals. The implied low contribution from chain conformational defects is in accordance with the low kink population found at room temperature for paraffins (Snyder *et al.*, 1983). Were such defects an important origin for the diffuse scatter, then the temperature dependence described above would not be observed.

The most interesting finding from this study is that a static longitudinal displacement exists for the long chain axes, even at low temperature, accounting well for the observed continuous diffuse scatter. In our model calculations, we used a r.m.s. displacement value of 0·25 Å, corresponding to a B_{33} quasi-thermal component of *ca* 5·0 Å^2. This finding contradicts earlier thermal studies on solution-crystallized *n*-paraffins, such as *n*-$C_{33}H_{68}$ (Strobl, Ewen, Fischer & Piesczek, 1974), for which such translational displacements are thought to be absent at low temperature. Such a longitudinal disorder in these microcrystals may result from the experimental condition that crystal growth occurred from a co-melt rather than from solution. By contrast, surface decoration of solution-grown microcrystals reveals that the surfaces are quite flat (Lotz & Wittmann, 1985) to support further this

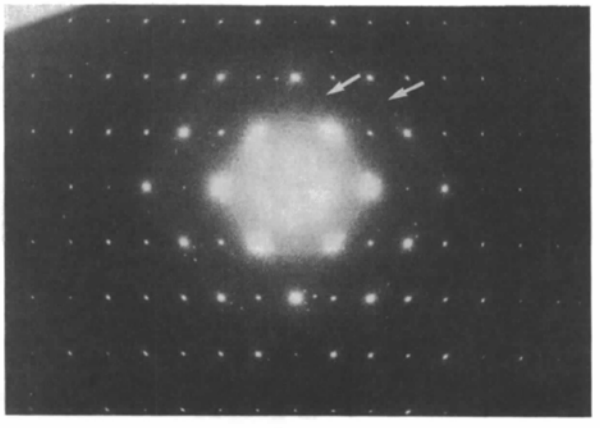

(*a*)

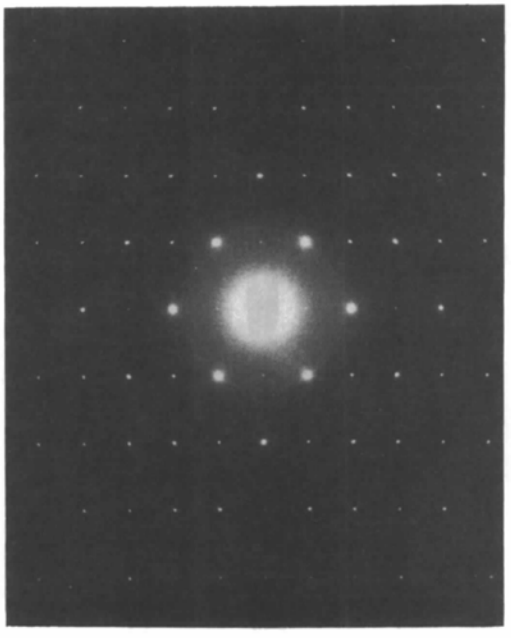

(*b*)

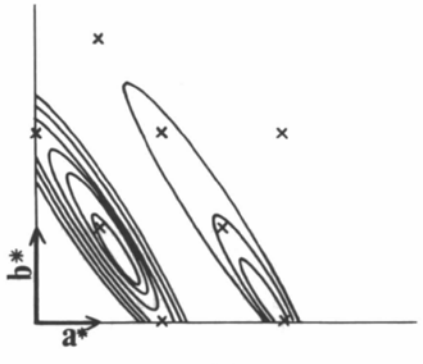

(*c*)

Fig. 4. Electron diffraction *hk*0 pattern from solution-grown microcrystals of *n*-$C_{36}H_{74}$ at (*a*) 296 K and (*b*) 150 K, showing that the diffuse component disappears at low temperature. [The diffuse scatter from a monolayer crystal is rather weak and difficult to reproduce in a photographic print. A clearer representation of this signal from a paraffin multilayer can be found in an earlier paper (Dorset, 1977)]. A good match to the observed pattern (*c*) is obtained from the TDS model in (1) when $B = 3$ Å^2. Although the kink defect or torsional disorder models also produce similar scattering motifs, their intensity is far lower than the thermal model due to the low defect content and/or angular distribution.

distinction. Thus, the longitudinal chain translation, favored at higher temperatures, can be frozen into the lattice as a distribution of static displacements. A small number of chain-end link defects, moreover, will guarantee that the lamellar interface will not, on average, deviate from a planar geometry.

Research was supported by a grant from the National Science Foundation (DMR8610783). The authors thank Dr Friedrich Zemlin for results obtained from the Suleika electron microscope.

References

ABRAHAMSSON, S., DAHLÉN, B., LÖFGREN, H. & PASCHER, I. (1978). *Progr. Chem. Fats Other Lipids*, **16**, 125-143.

AMORÓS, J. L. & AMORÓS, M. (1968). *Molecular Crystals. Their Transform and Diffuse Scattering*, p. 161. Wiley: New York.

ASBACH, G. J., GEIGER, K. & WILKE, W. (1979). *Colloid Polym. Sci.* **257**, 1049-1059.

BOYD, R. H. (1975). *J. Polym. Sci. Polym. Phys. Ed.* **13**, 2345-2355.

COCHRAN, W. (1956). *Acta Cryst.* **9**, 259-262.

CRAIEVICH, A., DOUCET, J. & DENICOLO, I. (1984). *J. Phys. (Paris)*, **45**, 1473-1477.

CRAVEN, B. M. & GUERINA, N. (1979). *Chem. Phys. Lipids*, **24**, 91-98.

DILL, K. A. & FLORY, P. J. (1980). *Proc. Natl Acad. Sci. USA*, **77**, 3115-3119.

DILL, K. A. & FLORY, P. J. (1981). *Proc. Natl Acad. Sci. USA*, **78**, 676-680.

DORSET, D. L. (1977). *Z. Naturforsch. Teil A*, **32**, 1161-1165.

DORSET, D. L., HANLON, J. & KARET, G. (1989). *Macromolecules*, **22**, 2169-2176.

DORSET, D. L., HOLLAND, F. M. & FRYER, J. R. (1984). *Ultramicroscopy*, **13**, 305-310.

DORSET, D. L., MOSS, B., WITTMANN, J. & LOTZ, B. (1984). *Proc. Natl Acad. Sci. USA*, **81**, 1913-1917.

DORSET, D. L., MOSS, B. & ZEMLIN, F. (1985-1986). *J. Macromol. Sci. Phys.* **B24**, 87-97.

GUINIER, A. (1963). *X-ray Diffraction in Crystals, Imperfect Crystals and Amorphous Bodies*. San Francisco: Freeman.

HEIDENREICH, R. D. (1964). *Fundamentals of Transmission Electron Microscopy*, p. 248. New York: Interscience.

HOPPE, W. (1964). *Advances in Structure Research by Diffraction Methods*, Vol. 1, edited by R. BRILL, pp. 90-166. New York: Interscience.

HU, H. & DORSET, D. L. (1989). *Acta Cryst.* **B45**, 283-290.

KIM, Y., STRAUSS, H. L. & SNYDER, R. G. (1989). *J. Phys. Chem.* **93**, 7520-7526.

LOTZ, B. & WITTMANN, J. C. (1985). *J. Microsc. Spectrosc. Electron.* **10**, 209-218.

MARONCELLI, M., QI, S. P., STRAUSS, H. L. & SNYDER, R. G. (1982). *J. Am. Chem. Soc.* **104**, 6237-6247.

MARONCELLI, M., STRAUSS, H. L. & SNYDER, R. G. (1985). *J. Chem. Phys.* **82**, 2811-2824.

SNYDER, R. G., MARONCELLI, M., STRAUSS, H. L., ELLIGER, C. A., CAMERON, D. G., CASAL, H. L. & MANTSCH, H. H. (1983). *J. Am. Chem. Soc.* **105**, 133-134.

STROBL, G., EWEN, B., FISCHER, E. W. & PIESCZEK, W. (1974). *J. Chem. Phys.* **61**, 5257-5264.

VAINSHTEIN, B. K. (1966). *Diffraction of X-rays by Chain Molecules*, p. 212. Amsterdam: Elsevier.

WITTMANN, J. C., HODGE, A. M. & LOTZ, B. (1983). *J. Polym. Sci. Polym. Phys. Ed.* **21**, 2495-2509.

Acta Cryst. (1991). A**47**, 549-553

Crystallography, Geometry and Physics in Higher Dimensions. X. Super Point Groups in Five-Dimensional Space for the Di-Incommensurate Structures

BY T. PHAN, R. VEYSSEYRE AND D. WEIGEL

Laboratoire de Chimie Physique du Solide (Unité de Recherche Associée au CNRS no. 453) et Laboratoire de Mathématique de la Physique, Ecole Centrale des Arts et Manufactures, Grande Voie des Vignes, 92295 Châtenay-Malabry CEDEX, France

(*Received* 26 *January* 1991; *accepted* 2 *April* 1991)

Abstract

This paper, the third of a series devoted to crystallography in five-dimensional space E^5, deals with the di-incommensurate structures. Physical considerations on the vectors of modulation have enabled the definition and listing of the di-incommensurate point symmetry operations, the di-incommensurate point symmetry groups and the di-incommensurate crystal families of the space E^5.

Introduction

A crystal lattice is said to be di-incommensurate (DI for short) if the vectors describing the main and satellite reflections may be labelled with five Miller indices as follows:

$$\mathbf{H} = h\mathbf{a}^* + k\mathbf{b}^* + l\mathbf{c}^* + m_1\mathbf{q}_1^* + m_2\mathbf{q}_2^* \qquad (1)$$

where h, k, l, m_1 and m_2 are integers and

$$\begin{aligned}\mathbf{q}_1^* &= \alpha_1\mathbf{a}^* + \beta_1\mathbf{b}^* + \gamma_1\mathbf{c}^* \\ \mathbf{q}_2^* &= \alpha_2\mathbf{a}^* + \beta_2\mathbf{b}^* + \gamma_2\mathbf{c}^*.\end{aligned} \qquad (2)$$

One at least of the three entries, α_1, β_1 and γ_1, is irrational, and also for the entries α_2, β_2 and γ_2. Then we can describe a reciprocal lattice in a (3+2)-

0108-7673/91/050549-05$03.00